ISSN 1512-1232

A NOVEL APPROACH FOR FINGERPRINT MATCHING USING DEFORMABLE MODEL FOR BETTER ALIGNMENT

Srinivasa Kumar Devireddy

St.Mary's Women's Engineering College,GunturA.P., India,
srinivaskumar_d@yahoo.com

Abstract

Fingerprint images are typically acquired using a contact-based sensor wherein a user places her finger on the surface of the sensor. The elastic nature of the human skin, coupled with the non-uniform pressure applied by the finger on the sensor, result in fingerprint images whose ridges exhibit non-linear distortions. For reliable matching, these non-linear distortion effects must be accounted for prior to comparing two fingerprint images. Models based on affine transformations have been used to offset the effects of distortion, but they invariably lead to unsatisfactory matching results since the distortions are basically elastic in nature.

Given several template impressions of a finger, we estimate the "average" deformation for each template image corresponding to that finger based on the thin plate spline (TPS) model.

The estimated average deformation is then utilized to align the minutiae points between the template and query images during the matching stage. It is shown that the use of an average deformation model leads to a better alignment between the two sets of points as opposed to a rigid transformation. The average deformation is computed using two types of landmark points: minutiae points and ridge points. Further, an index of deformation is proposed for choosing the best deformation model arising from a set of template impressions corresponding to a finger. Experimental data consists of 1600 fingerprints corresponding to 50 different fingers collected over a period of 2 weeks. It is shown that the average deformation model leads to an improvement in the alignment between impressions originating from the same finger.

Figure 1: Aligning two impressions of the same finger using an affine transformation. Due to non-linear distortions, the alignment is not accurate in some regions. Only fingerprint ridges are shown for clarity.

ISSN 1512-1232

1 Introduction

As indicated earlier, the problem of automatic fingerprint matching involves determining a measure of similarity between two fingerprint impressions by comparing their ridge structure and/or the spatial distribution of the minutiae points [3][4][5][6]. The image acquisition process, however, introduces non-linear distortions in the ridge structure and, consequently, in the spatial location of minutiae points, thereby confounding the matching process. This distortion is a function of several parameters including the orientation of the sensor with respect to the finger, the amount of pressure applied by the subject, the disposition of the subject (sitting or standing), the motion of the finger prior to its placement on the sensor, the moisture content of the skin (dry, oily or wet), the elasticity of the skin, etc. Therefore, the distortions observed in a fingerprint vary from one acquisition to the next. For reliable matching, these non-linear distortions must be accounted for prior to comparing two fingerprint images. Deformation models based on affine transformations invariably lead to unsatisfactory matching results since the distortions are basically elastic in nature (Figure 1).

To deal with the problem of non-linear distortion in fingerprint images, four types of approaches have been discussed in the literature. The first approach accounts for distortion in the image acquisition stage by capturing the least distorted print from the user. Ratha et al. [7] describe a system which does not accept an input image if the user applies excessive force on the sensor, thereby minimizing the effect of distortions on the acquired image. The system operates by measuring the forces and torques applied on the sensor. Dorai et al. [8] observe a video sequence of the fingertip as it interacts with the sensor and measure the distortion in successive frames. When excessive distortion is observed, the system requests the user to provide another fingerprint. These systems require specialized hardware and the ability to perform extensive computations in real-time. As a result, they do not offer a practical solution to fingerprint deformation for real-time and embedded fingerprint applications.

In the second approach, the distortion is estimated during the matching stage. Thebaud [9] uses a gradient descent technique to compute local warps when comparing two fingerprints. The fingerprint correlation score is used as the objective function. Besides being time consuming, this technique potentially results in a higher False Accept Rate (FAR) since it performs local warping to force a match between the two images. Kov´acs-Vajna [3] uses minutiae triplets to compare two minutiae sets. By not using the entire minutiae pattern at once, the cumulative effect of distortion is avoided. Bazen and Gerez [10] use a thin-plate spline (TPS) model to account for non-linear distortions while comparing two minutiae sets.

In the third approach, the distortion is removed before the matching stage. Senior and Bolle [11] have developed a model which assumes that ridges in a fingerprint are constantly spaced, and that deviations from this model indicate the presence of elastic distortions. They apply local warps in regions exhibiting such deviations to make the local ridge distances nearly equal the average inter-ridge spacing. Their experimental results show a significant improvement in genuine matching scores (i.e., the matching score when comparing two impressions of the same finger), as indicated by the t-statistic. However, their assumption that inter-ridge spacing in a fingerprint is constantly spaced is not always valid. Watson et al. [12] construct distortion tolerant filters for each (template) fingerprint before performing a correlation type of matching. Their experiments show that applying the filter before matching improves the performance.

ISSN 1512-1232

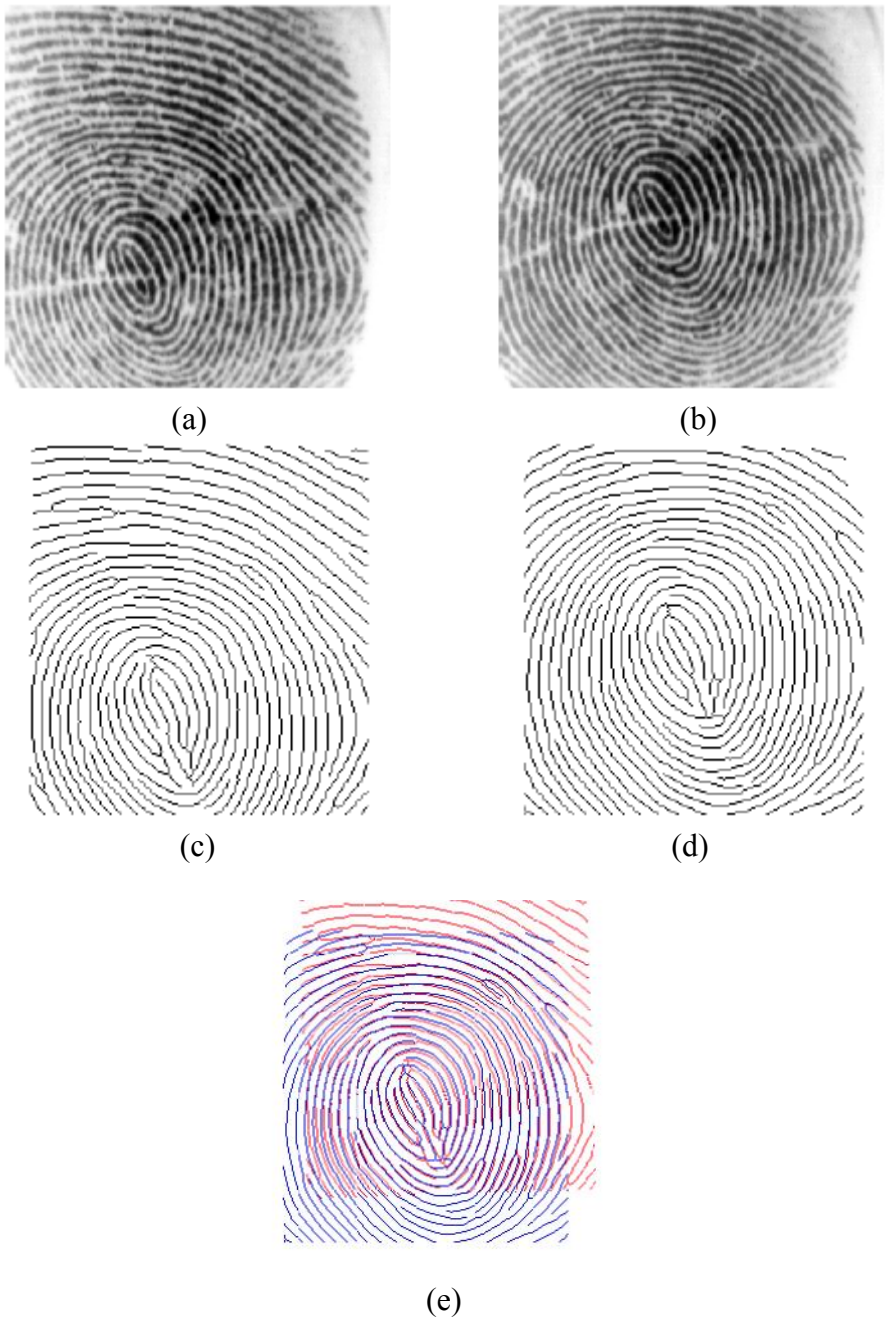

Figure 2: Alignment of two impressions of the same finger using affine transformation. (a) and (b) are the gray scale images; (c) and (d) are the thinned (skeletonized) images of (a) and (b), respectively; and (e) shows the alignment based on the thinned images. Ridge lines do not align in (e).

The fourth approach is more suited for introducing distortions in synthetic fingerprints. Cappelli et al. [13] have attempted to model the distortions that could occur in a fingerprint image by considering three concentric regions in a fingerprint; the inner and outer regions are assumed to have no distortions although ridges in the outer region can be translated and rotated with respect to the ridges in the inner region; the region in between is assumed to undergo non-linear distortions in order to accommodate the transition of ridges from the inner to the outer region. The authors, however, do not use this model to perform fingerprint matching. Rather, they use it to synthesize multiple impressions of the same finger [14].

Several difficulties arise when we try to ascertain the extent of non-linear distortion in fingerprint impressions. The distortion present in impressions of a finger is not known in advance, thereby making

ISSN 1512-1232

normalization to a true template as in [11] impossible. A reference template fingerprint having no distortion effects is never available given multiple impressions of a finger; in other words, distortion effects should appropriately be measured in relative, rather than in absolute, terms between pairs of impressions. Bazen and Gerez [10] report the estimation of relative distortions between pairs of impressions based on the minutiae point pattern correspondence (see Figure 3). In this paper, we present an approach of estimating relative distortions based on ridge curve correspondence (see Figure 4). Modelling distortion effects based on ridge curve correspondence offers several advantages over minutiae point pattern matching, consequently leading to improved authentication performance. Unlike minutiae points, which can be sparsely distributed in regions of a fingerprint image, ridge curves are spread all over the image domain resulting in a more reliable estimate of the distortion. The spatial continuity of ridge curves enables sampling of a large number of points on the ridges for establishing correspondences, including points in the vicinity of undetected minutiae points. Obtaining correspondences for undetected minutiae points is not possible when correspondences are based solely on (detected) minutiae point patterns. Also, in some poor quality images, minutiae information cannot be reliably extracted and thus, should not be used to construct a fingerprint distortion model. For the above reasons, ridge curve-based warping techniques result in a more robust and reliable estimate of the distortion in fingerprint impressions, and consequently, incorporating this distortion model in the authentication stage yields superior matching performance.

Most of the earlier techniques deal with the problem of non-linear distortion on a case by case basis, i.e., for every pair of fingerprint impressions, the distortion removal technique, via a deformation model, is applied and a matching score generated. No attempt has been made to develop a finger-specific deformation model that can be computed offline and later used for matching. The main advantage of such a scheme is that once a finger-specific model has been computed and stored along with the template, re-computation of the model is not necessary during the matching stage. When multiple impressions of a user's fingerprint are available, a technique is proposed for computing the average deformation model in the training stage using the thin plate spline (TPS) warping model based on ridge curve correspondence. The average deformation model corresponding to each fingerprint impression is an overall description of the relative distortions of the remaining impressions with that impression. In other words, we describe distortion effects by (i) a baseline impression and (ii) the average deformation model with respect to the baseline impression. An optimal baseline impression with the most consistent distortions is selected by means of an index of deformation. The optimal baseline impression is not an impression with no distortion effects; it is the impression relative to which other impressions of the same finger have the most consistent distortions. We show that by removing distortion effects using the optimal baseline impressions, superior matching performance is obtained in the authentication stage.

2 General Warping Methods

Warping methods can be used to obtain global deformation models for image registration. Applications of warping techniques abound in the statistical, medical imaging and computer vision literature. There have been a variety of image registration techniques motivated from different principles; examples include warping by elastic deformations [15][16], optical or fluid flow [17][18][19], diffusion processes [20], Bayesian prior distributions [21][22], and thin-plate splines (TPS) [23][24][25]. Only recently have warping techniques based on deformation models been used to model distortions in fingerprint images for the purpose of matching [26][10]. Warping enables the distortions to be estimated and subsequently removed prior to matching. It is shown in [10] that this procedure results in superior matching performance compared to algorithms which either do not model distortions or model them using rigid transformations. Distortion models based on TPS were used in [26] and [10].

ISSN 1512-1232

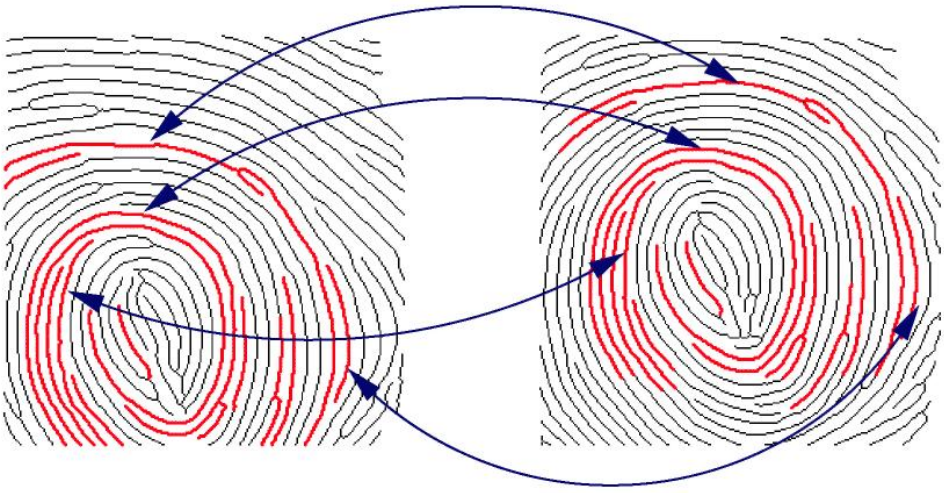

Figure 3: An example of minutiae correspondences between two impressions of a finger.

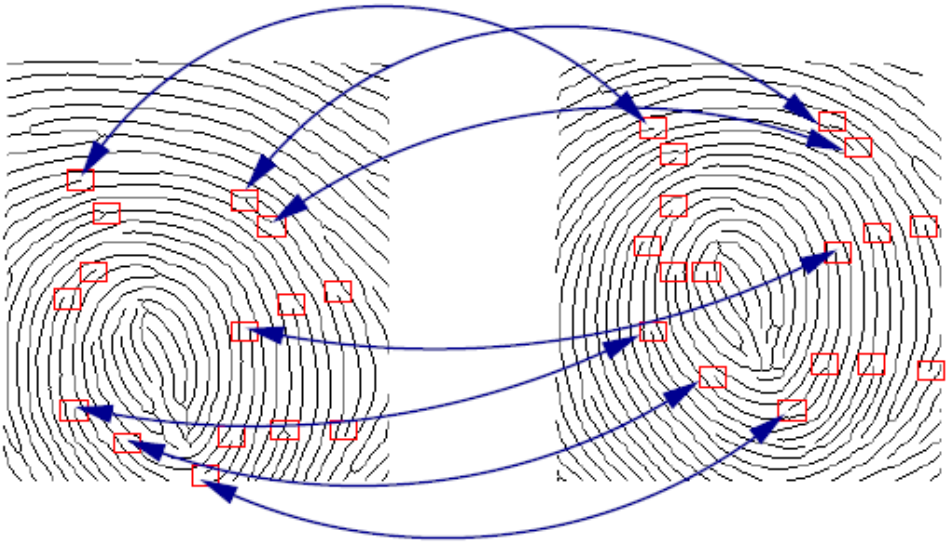

Figure 4: An example of ridge curve correspondences between two impressions of a finger.

Earlier work in modelling the non-linear distortion in fingerprint images used only the spatial distribution of the minutiae points [26][10]. One disadvantage of using the minutiae point pattern for estimating the non-linear deformation is that minutiae points may be sparse in some areas of the fingerprint. A more fundamental and rich feature of fingerprint images is their ridge structure. A skeletonized version of a fingerprint image, known as the thinned image, can be used to extract ridge curve information (see Figure 2). Obtaining the deformation model based on aligning the ridge curves offers several advantages. Firstly, ridge lines are distributed over the entire fingerprint image and thus, a more reliable deformation model can be obtained. Secondly, the likelihood of incorrectly corresponding two ridge curves is much less than corresponding two minutiae points, due to the richer intrinsic information available in curves compared to points. Consequently, the deformation model based on ridge curves yields better matching performance compared to minutiae points as is shown in this paper.

When multiple impressions of a finger are available, it is observed that the nonlinear distortion present in them vary significantly. Further, these distortions are different for different pairings of the impressions (Figure 5).

ISSN 1512-1232

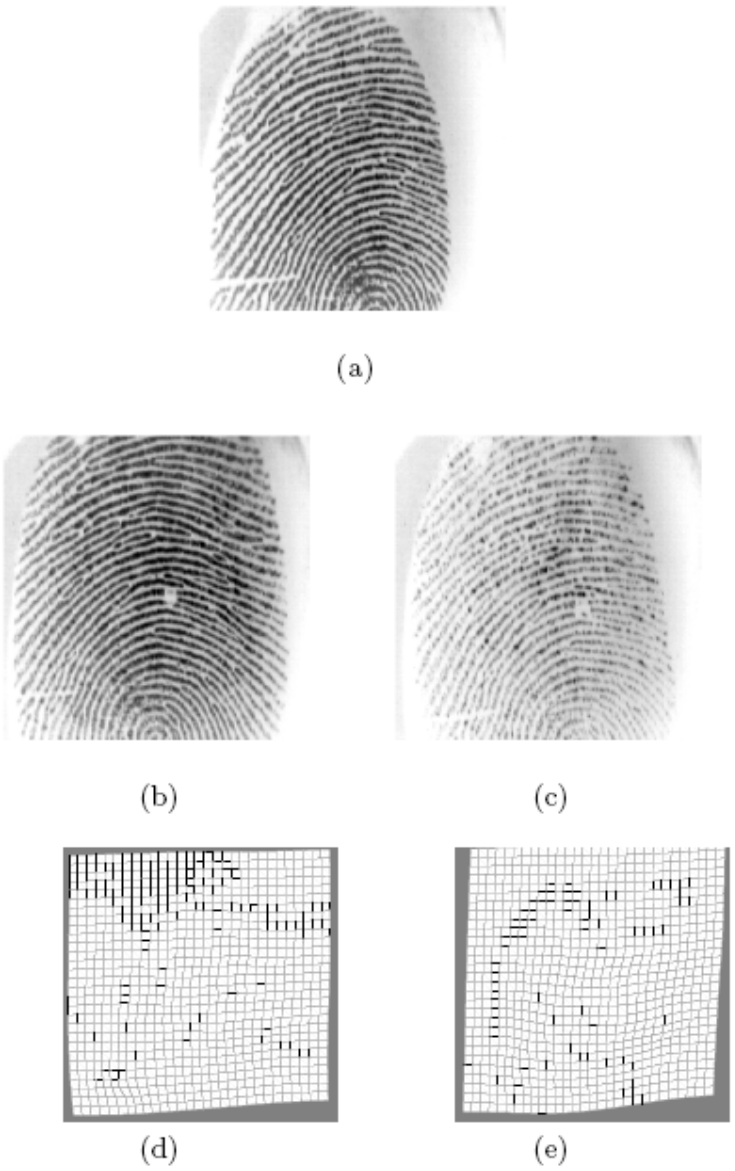

Figure 5: Non-linear deformations (with rotation and translation parameters removed) associated with two pairings involving the same template: (a) Template image; (b) and (c) Query images; (d) and (e) Non-linear deformation of (a) into (b) and (c), respectively.

Thus, we address the following two problems: (i) obtain a deformation model based on ridge curve correspondence that can be incorporated in the matching stage, and (ii) given multiple deformation models for a finger, select the optimal model that gives the most consistent distortion effects measured from a baseline impression. In this paper, we develop an *average* deformation model given multiple impressions of a single finger together with an estimate of its variability based on ridge curve correspondences. An index of deformation is suggested as a means of selecting a baseline impression with an associated average deformation model with the least variability. The average deformation model is incorporated in the matching stage when a query fingerprint is compared against a template fingerprint. Experimental results indicate that better matching performance is achieved by incorporating deformation models (and average deformation models) based on ridge curves as opposed to using only minutiae points.

ISSN 1512-1232

3 The Fingerprint Warping Model

Let $I_0(x,y)$ and $I_1(x,y)$ denote two fingerprint impressions, where $(x,y) \in S$ for a domain $S \subset R^2$. Our convention is to refer to I_0 and I_1 as the template and query images, respectively. A warping of I_0 to I_1 is defined as the function $F : S \rightarrow S$ such that

$$I_0(F(x,y)) = I_1(x,y) \qquad (1)$$

for $(x,y) \in S$. The function F is called the warping function which takes I_0 to I_1. In our application we register the two impressions I_0 and I_1 by matching corresponding ridge curves. Thus, in equation (5.1), the warping function, $F : S \rightarrow S$, registers two sets of ridge curves derived from I_0 and I_1. Let $u_k \equiv u_k(t) = (u_{k1}(t), u_{k2}(t))^T, t \in C_k,$ denote a parameterized ridge curve in I_0 for $k = 1, 2,..., n,$ and let $v_k \equiv v_k(t) = (v_{k1}(t), v_{k2}(t))^T, t \in D_k$ and $k = 1, 2, \ldots, n,$ denote the corresponding parameterized ridge curves in I_1; here, n is the total number of corresponding curves. The two sets of ridge curves, one set in I_0 and the other in I_1, with known correspondences is denoted by the pair (U, V) where $U = (u_1, u_2, ..., u_n)^T$ and $V = (v_1, v_2, .., v_n)^T$. We assume that each correspondence pair is aligned as close as possible using rigid transformation prior to non-linear warping. This can be achieved using the Procrustes analysis (see [27]) after pairs of corresponding points are obtained using the methodology outlined below. For n pairs of ridge curve correspondences, a warping function, F, that warps U to V, subject to perfect alignment, is given by the conditions

$$F(u_k) = v_k \qquad \text{for k=1,2,.....n.} \qquad (2)$$

3.1 Establishing Ridge Curve Correspondences

Given a pair of grayscale fingerprint images, I_0 and I_1, we obtain their thinned versions, R_0 and R_1, using the algorithm described in [1]. A thinned image is a binary image (see Figures 2 (c) and (d)) with grayscale values of 0 (indicating ridges) and 255 (indicating valleys). Each thinned image can be thought of as a collection of ridge curves. In order to develop ridge curve correspondences, we proceed as follows:

1. Minutiae points are extracted from I_0 and I_1 using the algorithm described in [13]. Let $M_0 = (m_{0,1}, m_{0,2}, ..., m_{0,k_0})$ and $M_1 = (m_{1,1}, m_{1,2}, ..., m_{1,k_1})$ denote the two minutiae sets of cardinalities K_0 and K_1, respectively. Here, each minutiae point $m_{i,j}$ is characterized by its location in the image, the orientation of the associated ridge, and the grayscale intensity of pixels in its vicinity.
2. Minutiae correspondences between M_0 and M_1 is obtained using the elastic string matching technique described in [2]. The output of the matcher is a similarity score in the range [0,1000] and a set of correspondences of the form $C = \{(m_{0,a_j}, m_{1,b_j}) : j = 1, 2, ..., K\}$ where $K \leq \min\{K_0, K_1\},$ and the a_js $(b_j$s$)$ are all distinct. Figure 5.3 shows an example of the minutiae point pattern correspondence for two impressions of a finger.

ISSN 1512-1232

3. Once the correspondence between M_0 and M_1 is established, the ridge curves associated with these minutiae points are extracted from R_0 and R_1 using a simple ridge tracing technique. A minutiae point that is a ridge ending has one ridge curve associated with it while a ridge bifurcation has three associated ridges. In the case of a ridge ending, the ridge curve correspondence between the two images can be easily established since each minutiae point has only one associated ridge curve. However, in the case of a ridge bifurcation, the problem of establishing ridge curve correspondences is non-trivial due to the presence of multiple ridge curves for each minutiae point; each of the three component ridge curves of one minutiae point can potentially match with any component of the other impression.

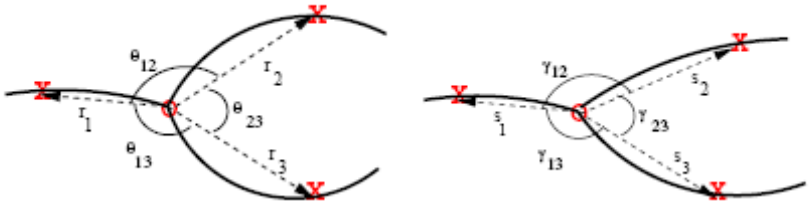

Figure 6: Vector representation of ridge bifurcation used to establish correspondences between component ridge curves. *O* marks the bifurcation points in correspondence, and *X* marks the points on the ridges at Euclidean distance *d* from *O*.

To resolve this ambiguity, each ridge curve corresponding to the minutiae point in $I_0\,(I_1)$ is represented as a directional vector $r_j(s_j),\ j=1,2,3,$ based on two points on the ridge curve: the minutiae point and the *d-th* point *(d* = 20) on the ridge from the minutiae (see Figure 6). We define $\theta_{j,k}\,(\gamma_{j,k})$ to be the angle that $r_j\,(s_j)$ makes with $r_k\,(s_k),$ for $k \neq j$. We find the vector $r_j\,(s_j)$ for which the angles $\{\theta_{j,k}, k \neq j\}$ $(\{\gamma_{j,k}, k \neq j\})$ are both obtuse. This establishes the first ridge curve correspondence, say, $r_1 \square s_1,$ without loss of generality. We then compute the cross products $c_r = r_2 \times r_3$ and $c_s = s_2 \times s_3$. We assign the correspondence $r_2 \square s_2$ and $r_3 \square s_3$ if c_r and c_s are of the same sign, and $r_2 \square s_3$ and $r_3 \square s_2$, otherwise. Figure 5.4 shows an example of ridge curve correspondence for a pair of impressions of a finger.

3.2 Sampling Ridge Curves

Having determined the corresponding ridge curves, we next establish a correspondence between *points* on these curves by sampling every q*-th* point *(q* = 20) on each of the ridge curves. For the correspondence pair *(U, V),* we have $u_k \equiv u_k(t)$ and $v_k \equiv v_k(t)$ for *k* = 1,2,..., n. The sampling of the k-th corresponding ridge curves, say at points $t_1, t_2, \ldots, t_{g_k}$, yields g_k pairings of the form $(u_k(t_j), v_k(t_j))$ for *j* = 1, 2,..., g_k. Thus, we have a total of $N = \sum_{k=1}^{n} g_k$ points in establishing the correspondence. We denote this set of corresponding points by *U* = (n^, n*,..., $n^*_M)^T$ and V = (So, E|, . . ., ^)^T). We use TPS to estimate the non-linear deformation *F* based on these points. TPS represents a natural parametric generalization from rigid to mild non-rigid deformations. The deformation model for TPS is given in terms of the warping function *F(u),* with

$$F(u) = c + A.u + W^T s(u), \qquad (3)$$

ISSN 1512-1232

where $u \in S$, c is a 2×1 translation vector, A is a 2×2 affine matrix, W^{T} is a $\mathrm{N}\times2$ coefficient matrix, $\mathrm{s}(\mathrm{u}) = (\sigma(\mathrm{u}-\mathrm{u}_1^*), \sigma(\mathrm{u}-\mathrm{u}_2^*), \ldots, \sigma(\mathrm{u}-\mathrm{u}_{\mathrm{N}}^*))^{\mathrm{T}}$ where

$$\sigma(u) = \begin{cases} \|u\|^2 \log(\|u\|) & \|u\| > 0 \\ 0, & \|u\| = 0 \end{cases} \qquad (4)$$

In equation (3), there are 6 and *2N* parameters corresponding to the rigid and non-rigid parts of the deformation model, respectively, resulting in a total of 2N + 6 parameters to be estimated. The restrictions

$$F(u_j^*) = v_j^*, \qquad \text{for j=1,2,....,} \qquad (5)$$

j = 1, 2,...,N provide *2N* constraints. For the parameters to be uniquely estimated, we further assume that W satisfies the two conditions (i) $1_{\mathrm{N}}^{\mathrm{T}}\mathrm{W} = 0$ and (ii) $\mathrm{U}_{\mathrm{s}}^{\mathrm{T}}\mathrm{W} = 0,$ where 1_N is the vector of ones of length N. Thus, the parameters of the TPS model can be obtained from the matrix equation

$$\begin{bmatrix} H & 1_N & u \\ 1_N^T & 0 & 0 \\ u^T & 0 & 0 \end{bmatrix} \begin{bmatrix} W \\ c^T \\ A^T \end{bmatrix} = \begin{bmatrix} v \\ 0 \\ 0 \end{bmatrix}, \qquad (6)$$

where H is the $N \times N$ matrix with entries $\mathrm{h}_{\mathrm{i,j}} = \sigma(\mathrm{u}_{\mathrm{i}}^* - \mathrm{u}_{\mathrm{j}}^*).$

The matrix equation in (6) gives rise to a TPS model that minimizes the bending energy subject to the perfect alignment constraints in (5). A more robust TPS model can be obtained by relaxing the constraints in equation (5), and instead determining the function F which minimizes the expression

$$\sum_{j=1}^{N} (v_j^* - F(u_j^*))^T (v_j^* - F(u_j^*)) + \lambda J(F), \qquad (7)$$

Where

$$J(F) = \sum_{j=1}^{2} \int_s \left\{ \left(\frac{\partial^2 F_j(x,y)}{\partial x^2} \right)^2 + 2\left(\frac{\partial^2 F_j(x,y)}{\partial x \partial y} \right)^2 + \left(\frac{\partial^2 F_j(x,y)}{\partial y^2} \right)^2 \right\} dxdy \qquad (8)$$

represents the bending energy associated with $\mathrm{F} = (\mathrm{F}_1, \mathrm{F}_2)^{\mathrm{T}}, \mathrm{F}_{\mathrm{j}}$ is the j^{th} component of F, and $\lambda > 0$. The case $\lambda = 0$ gives rise to the TPS model described by equation (6). For general $\lambda > 0$, the parameters of the resulting TPS model can be obtained using equation (6) with H replaced by $\mathrm{H} + \lambda \mathrm{I}_{\mathrm{N}},$ where I_{N} is the $N \times N$ Identity matrix.

ISSN 1512-1232

4 Average Deformation Model

Suppose we have *L* impressions of a finger, $T_1, T_2, \ldots, T_L$. Each impression, T_i, can be paired with the remaining impressions, $T_j, j \neq i$, to create $L-1$ pairs of the form (T_i, T_j). For the pair (T_i, T_j), we obtain a non-linear transformation F_{ij} by employing the technique described in section 5.3. Note that F_{ij} transforms *every* pixel in the template fingerprint, T_i, to a new location. Thus, we can compute the *average* deformation of each pixel u in T_i as

$$\overline{F}_i(u) = \frac{1}{L-1} \sum_{j \neq i} F_{ij}(u), \qquad (9)$$

There will be *L* average deformation models corresponding to the *L* impressions of the finger. The average deformation is the typical deformation that arises when we compare one fingerprint impression of a finger (the baseline impression) with other impressions of the same finger. Figure 7 shows that changing the baseline impression for the finger will result in a different average deformation model for that finger (the Φ values are as discussed in section 4.1). Figure 8 shows the average deformation for 3 different fingers; it can be clearly seen that the average warping functions are different for the 3 fingers indicating that the fingerprint deformation is finger-specific.

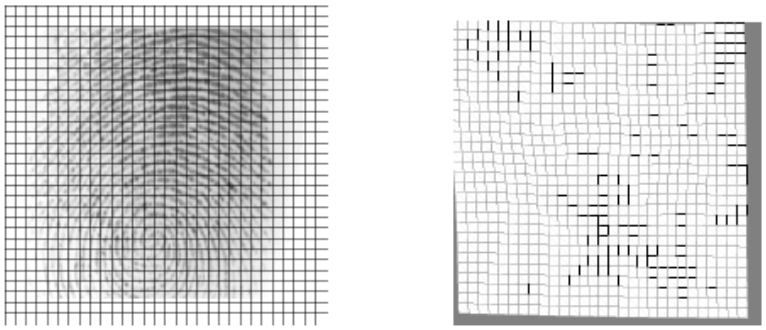

(a) $\Phi = 15.54$

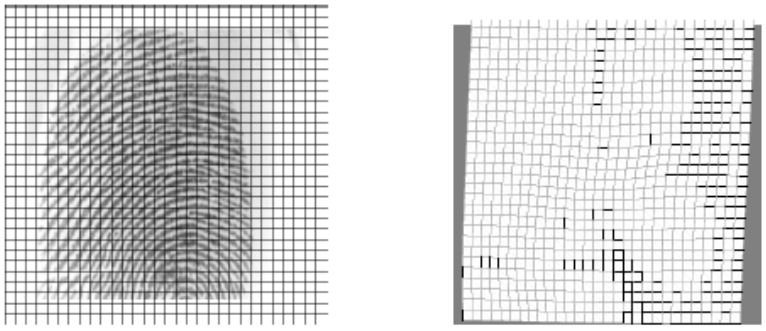

(b) $\Phi = 17.97$

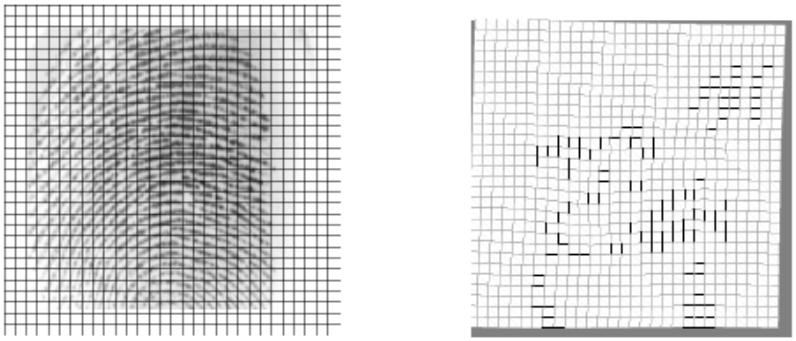

(c) $\Phi = 48.79$

ISSN 1512-1232

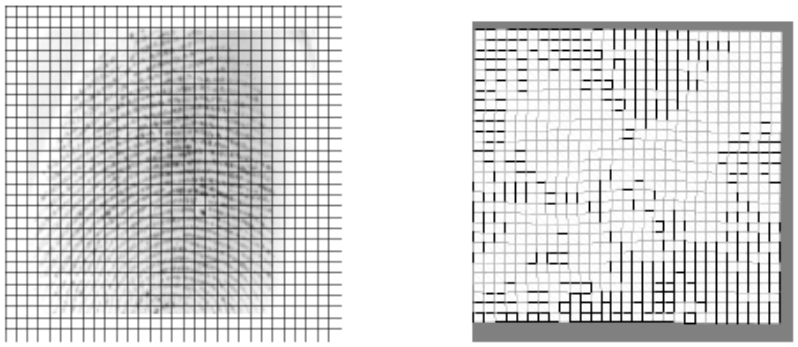

(d) $\Phi = 83.12$

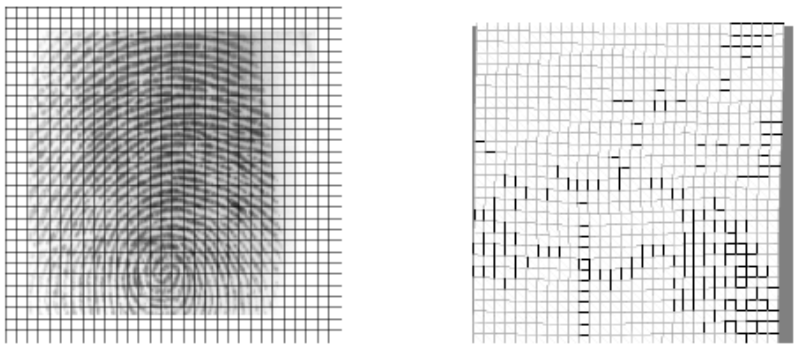

(e) $\Phi = 94.34$

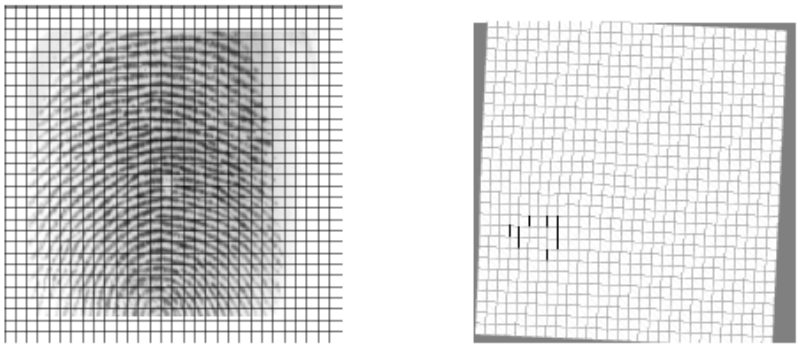

(f) $\Phi = 232.53$

Figure 7: The average deformation model (shown as deformations on a reference grid) corresponding to 6 templates of a finger sorted in increasing Φ-values. (a) is chosen to be the optimal template since it has the least Φ-value.

ISSN 1512-1232

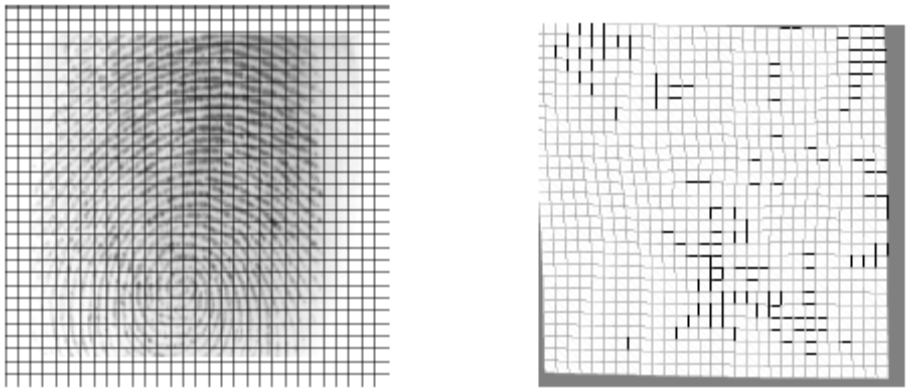

(a) $\Phi = 46.68$

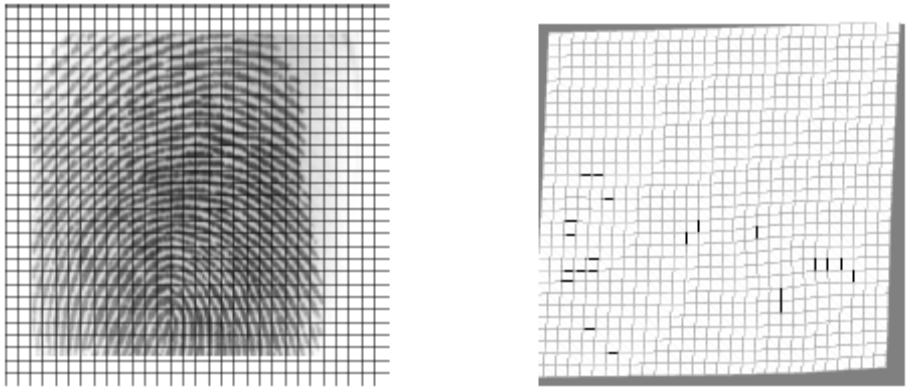

(b) $\Phi = 37.59$

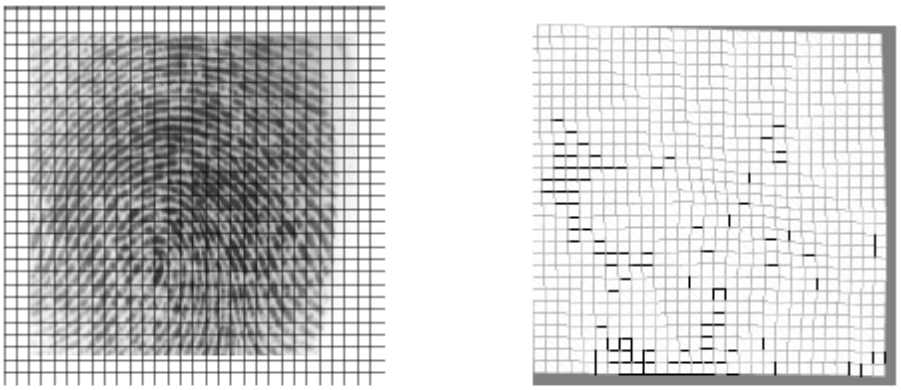

(c) $\Phi = 85.18$

Figure 8: The average deformation model (shown as deformations on a reference grid) of 3 different fingers .

4.1 The Φ Index of Deformation

We consider the following two questions in this section:

1. Which of the *L* average deformation models can be considered to be the optimal model for this finger?
2. Will the optimal model, when incorporated in the matching stage, result in improved performance compared to the suboptimal models?

ISSN 1512-1232

In order to address these questions, we first define the pixel-wise covariance matrix associated with the i-th average deformation, $\overline{F_i}$, as follows:

$$D_{\overline{F_i}}(u) = \frac{1}{L-1}\sum_{j \neq i}\left(F_{ij}(u) - \overline{F}_i(u)\right).\left(F_{ij}(u) - \overline{F}_i(u)\right)^T \qquad (10)$$

where F_{ij} is the deformation function that warps T_i to T_j. The covariance matrix defined at each pixel *u,* is a measure of the variability associated with the estimated deformation functions. Two choices of pixel-wise measures of variability are given by (i) the determinant, $\phi(D_{\overline{F_i}}(u)) = \left|D_{\overline{F_i}}(u)\right|$, and (ii) the trace, $\phi(D_{\overline{F_i}}(u)) = \mathrm{tr}(D_{\overline{F_i}}(u))$. Pixels with large (small) values of ϕ indicate high (low) variability in the deformations F_{ij}. We propose to use the values of ϕ to determine the optimal model for a given finger. We define the i^{th} index of deformation, Φ_i, as

$$\Phi_i = \frac{1}{|S|}\sum_{u=1}^{|S|}\phi\left(D_{\overline{F}_i(u)}\right), \qquad (11)$$

where, $\phi(D) = \mathrm{tr}(D)$, and $|S|$ is the number of pixels in the domain *S*. Subsequently, we choose T_{i^*} as the template with the smallest variability in deformation if $i^* = \arg\min_i \Phi_i$. In effect, we choose that template T_i that minimizes the average variation across pixels measured in terms of Φ_i. Low (high) values of the index of deformation indicate that the warping functions are similar (dissimilar) to each other.

4.2 Eliminating Erroneous Correspondences

For each baseline fingerprint impression, it is important to determine the set of minutiae points that are correctly paired to form a correspondence. The reason for this is that the average deformation model is sensitive to the accuracy of the ridge curve correspondence, which in turn depends on the minutiae correspondence. It is, therefore, necessary to check the correctness of the minutiae correspondences prior to obtaining the ridge curve correspondences. Figure 9(a) gives an example of two incorrect minutiae correspondences which result in incorrect ridge curve correspondences (Figure 9(b)). These erroneous correspondences have to be eliminated prior to computing the average deformation model; failure to exclude such minutiae points results in a warping model that exhibits spurious distortions. This is done using the technique described below.

For the given baseline fingerprint impression, minutiae points that have a correspondence with at least $\ell\,(\ell = 5)$ of the remaining *L* - 1 impressions are extracted. We denote the set of all extracted minutiae points by $M = \{m_i, i = 1, 2, \ldots, K\}$, where *K* is the total number of such minutiae points. Each m_i has a corresponding minutie point in at least ℓ of the L-1 impressions.

ISSN 1512-1232

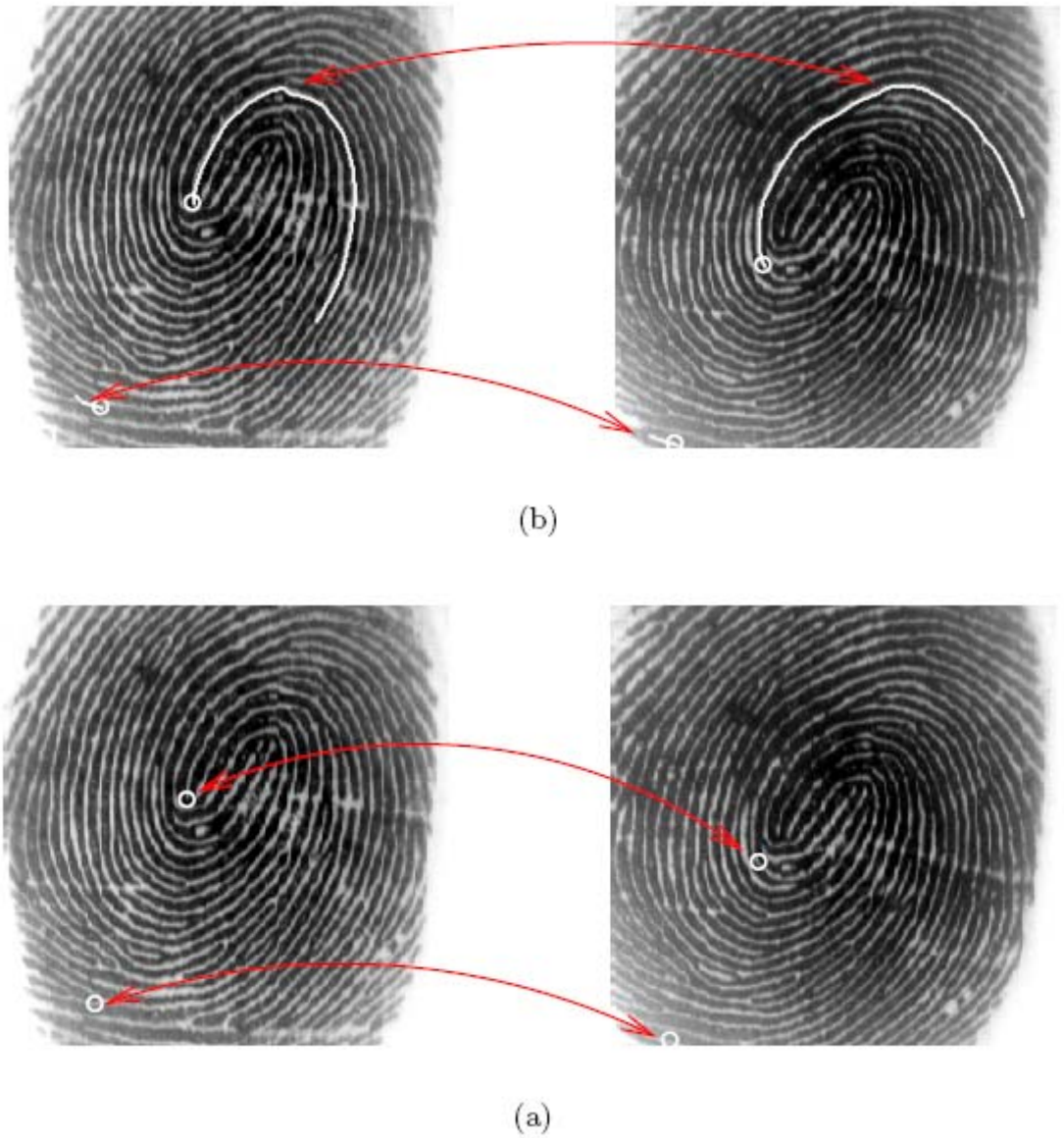

Figure 9: Examples of incorrect minutiae correspondences (a) resulting in erroneous ridge curve correspondences (b).

ISSN 1512-1232

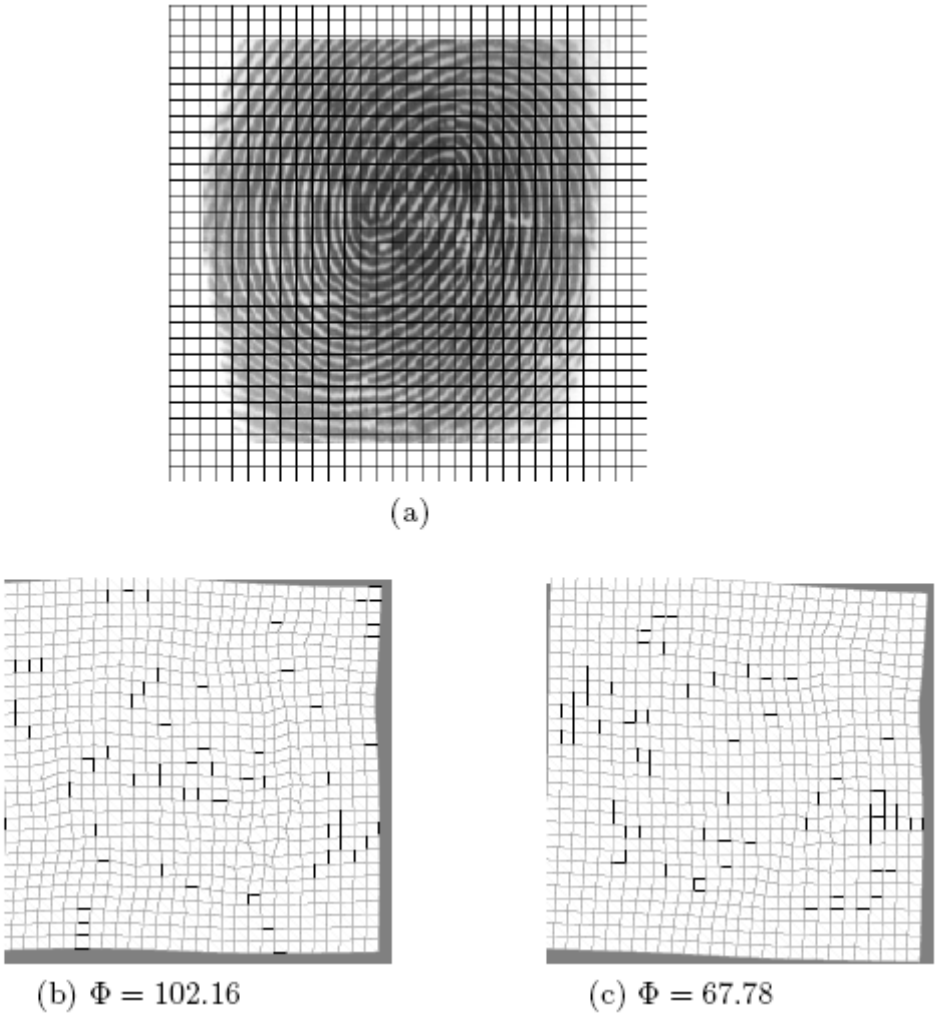

Figure 10: Effect of eliminating unreliable minutiae correspondences on the average deformation model; (a) template fingerprint, (b) average deformation model with p = 100, and (c) average deformation model with p = 60.

We denote these pairings by $(m_i, p_1), (m_i, p_2), \ldots, (m_i, p_{\ell_i})$, where ℓ_i is the total number of pairings. We now develop a measure of reliability for minutiae point mi as follows:

1. Sampled ridge point correspondences are obtained for each $(m_i, p_j), j = 1, 2, \ldots, n_i$ based on which a TPS deformation model, $F_{(m_i, p_j)}$ is computed. The average deformation model for the minutiae point m_i is given by

$$\overline{F}_{m_i}(u) = \frac{1}{\ell_i} \sum_{j=1}^{\ell_i} F_{(m_i, p_j)}(u)$$

Here, the average deformation model is obtained in a 10 x 10 square region, say S_{m_i}, centered at m_i.

2. Let

ISSN 1512-1232

$$D_{\overline{F}_{m_i}}(u) = \frac{1}{l_i}\sum_{j=1}^{l_i}(F_{(m_i,p_j)}(u) - \overline{F}_{m_i}(u)).(F_{(m_i,p_j)}(u) - \overline{F}_{m_i}(u))^T \qquad (12)$$

denote the site-wise variability measure of the deformations $F_{(mi,pj)}$ around F_{mi}. The average variability is measured by

$$R_{m_i} = \frac{1}{|S_{m_i}|}\sum_{u=1}^{|S_{m_i}|} trace(D_{\overline{F}_{m_i}}(u))$$

with small values of R_{m_i} indicating better reliability. Correspondences pertaining to those minutiae points with R_{m_i} values lower than the p-th percentile (e.g., p = 60) are used to develop the average deformation model for the template fingerprint.

For the incorrect minutiae correspondences in Figure 9, the value of R for the top minutiae point was 93.2 (the 60-th percentile value of R was 55.5 for this template) while the lower minutiae point occurred in less than 5 corresponding pairs and hence was eliminated. Figure 10(a) shows the average deformation model that results for this template when all correspondences are used (i.e.,p = 100); Figure 10(b) gives the deformation model for p = 60.

5 Experimental Results

In order to apply the TPS model to reliably estimate fingerprint deformation, we need to have several impressions of the same finger. Large number of impressions of a finger are not available in standard fingerprint databases (e.g., FVC 2002 [28]). Therefore, fingerprint images of 50 fingers were acquired using the Identix sensor (256 x 255, 380 dpi) over a period of two weeks in our lab. There were 32 impressions corresponding to every finger, resulting in a total of 1600 impressions. One half of the impressions (L = 16 for each finger, resulting in 800 impressions) were used as templates to compute the average deformation model for each finger, while the remaining 800 impressions were used as query images for testing. For each template image, T, the minutiae set, M_T, and the thinned image, R_T, were extracted. The average deformation model of T, $\overline{F_T}$, was obtained based on pairings with the remaining 15 impressions of the same finger (equation (7) with λ = 0.1). The minutiae set M_T was transformed to the deformed set, $MD_T \equiv \overline{F_T}(M_T)$ using $\overline{F_T}$. A total of 800 sets (50 x 16) of deformed minutiae points were thus obtained. In order to test the matching performance of the deformed minutiae sets, and the utility of the index of deformation, Φ, the following two experiments were conducted. In both these experiments, the minutiae matcher described in [2] was used to generate the matching (similarity) score.

In the first experiment, the matching performance using the average deformation model was evaluated. Every template image, T, was compared with every query image, Q, and two types of matching scores were generated for each comparison: the matching score obtained by matching (i) M_T with M_Q, and (ii) MD_T with M_Q. The Receiver Operating Characteristic (ROC) curve plotting the genuine accept rate (GAR) against the false accept rate (FAR) at various matching thresholds is presented in Figure 12. An overall improvement of 2% is observed when the average deformation model is used to distort M_T prior to matching.

ISSN 1512-1232

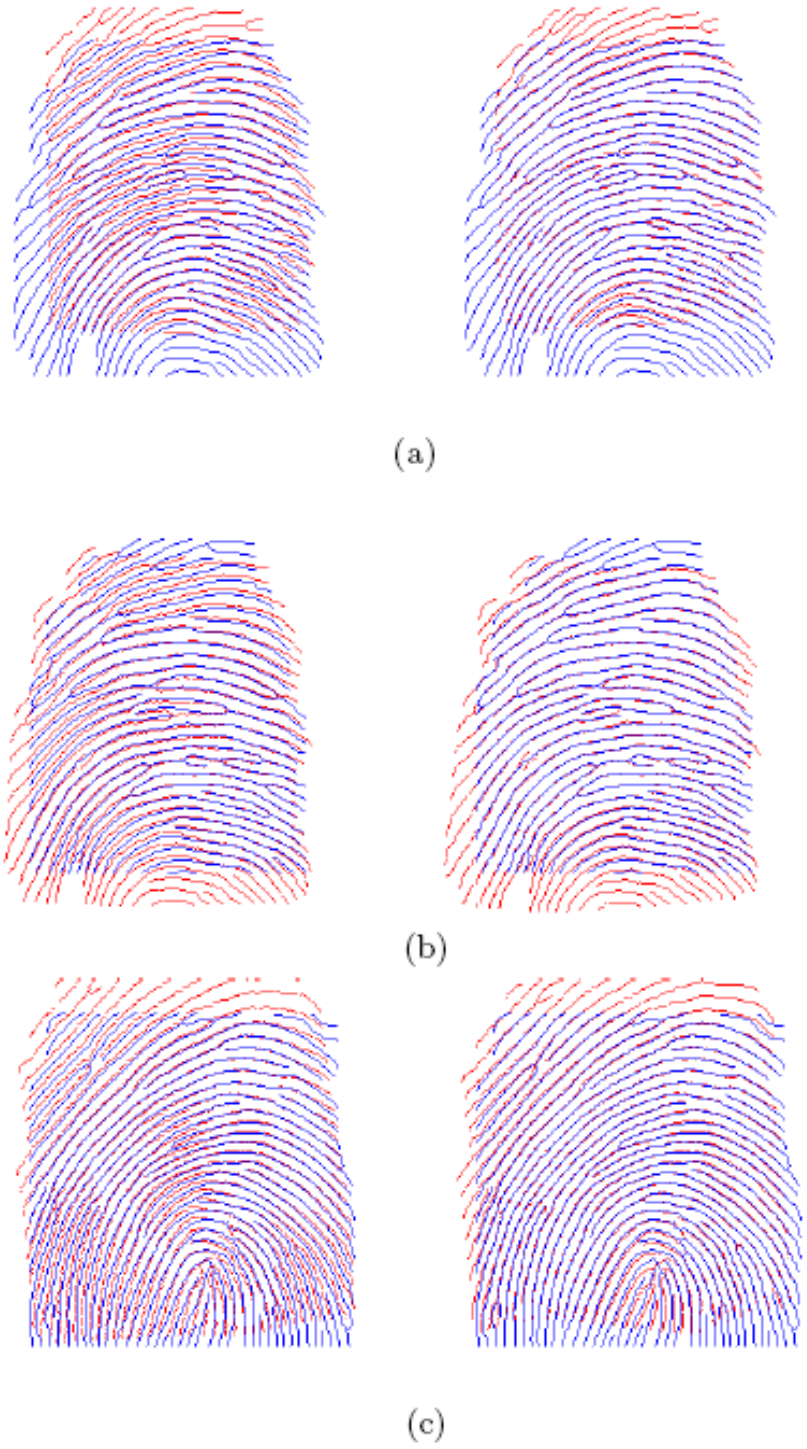

Figure 11: Improved alignment of template and query images using ridge curve correspondences (right panel). The alignment using minutiae correspondences are shown in the left panel. Both sets of alignment use the TPS warping model.

ISSN 1512-1232

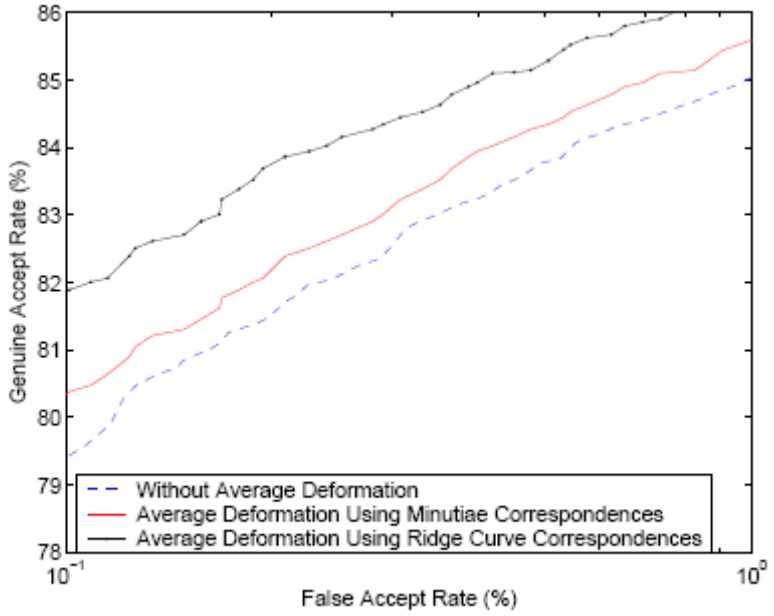

Figure 12: Improvement in matching performance when ridge curve correspondences is used to develop the average deformation model.

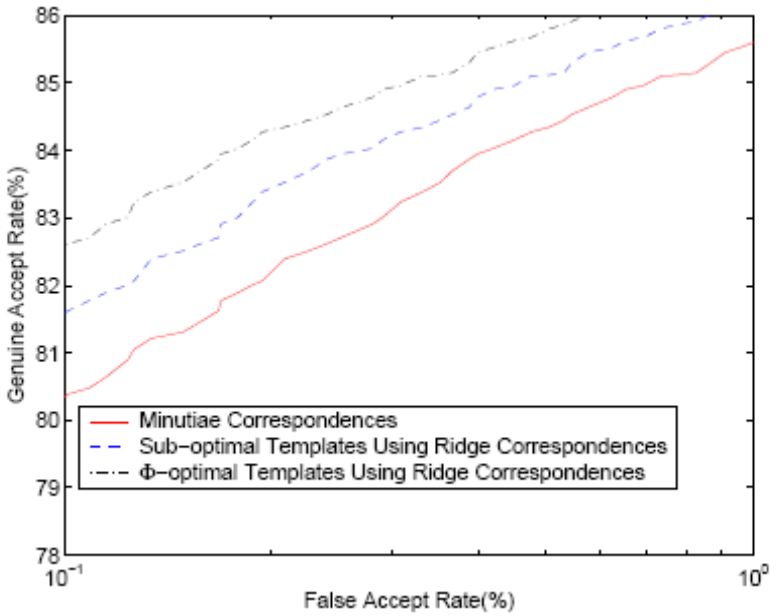

Figure 13: Matching performance when the Φ index of deformation is used to select optimal templates. Both optimal and suboptimal templates using ridge curve correspondences result in superior matching performance compared to minutiae correspondences.

In the second experiment, the advantage of using the index of deformation is demonstrated. The Φ-index of deformation (with $\phi(D) = tr(D)$) of every template image is used to rank the templates according to their variability in the distortion. The template images can now be split into two sets: (i) impressions with the least Φ values for every finger (the Φ-optimal templates) and (ii) the remaining impressions for every finger (the Φ-suboptimal templates). We repeated the matching procedure outlined above using these two template sets. The resulting ROC curve is shown in

ISSN 1512-1232

Figure 13. From the figure, it is clear that using Φ-optimal templates results in better performance compared to using Φ-suboptimal templates. Further, the Φ-suboptimal templates still yield better performance compared to the non-distorted templates thus demonstrating the importance of the average deformable model.

6. Conclusion

In this Paper, a deformation model for estimating the distortion effects in fingerprint impressions has been proposed. The distortion is computed based on ridge curve correspondence. It has been shown that the deformation model based on ridge curve correspondence gives superior authentication performance compared to minutiae point pattern matching. The warping model samples the ridge curve and uses thin-plate splines for estimating the non-linear deformation. An index of deformation has also been proposed for selecting the "optimal" template from a given set of fingerprint impressions.

The work presented here can be expanded in several ways. An interesting exercise would be to design an incremental approach to updating the average deformation model, i.e., updating the current average deformation model of a finger by using information presented by newly acquired fingerprint impressions. The technique proposed here uses a simple pixel-wise averaging measure to compute the average deformation model. This measure is sensitive to extreme deformations borne out by outliers; thus, more robust measures of describing the finger specific average deformation model are needed. The effect of the number of training samples (used to develop the average deformation model) on the matching performance has to be systematically studied.

Non-linear deformation in fingerprints is a consequence of utilizing contact-based sensors for imaging the fingertip. Using an acoustic (ultrasound) camera to procure fingerprint images may help avoid this problem [29]. However, an ultrasound camera introduces other challenges that may affect the quality of the image (e.g., a high quality reconstruction procedure is required to "assemble" an image). Further, the cost of the camera and its size may limit its deployment in real-world applications.

REFERENCES

1. A. K. Jain, R. Bolle, and S. Pankanti, eds., Biometrics: Personal Identification in Networked Society. Kluwer Academic Publishers, 1999.
2. A. K. Jain, L. Hong, and R. Bolle, "On-line fingerprint verification," IEEE Transactions on PAMI, vol. 19, pp. 302–314, April 1997.
3. Z. M. Kov´acs-Vajna, "A fingerprint verification system based on triangular matching and dynamic time warping," IEEE Transactions on PAMI, vol. 22, pp. 1266–1276, Nov 2000.
4. D. Roberge, C. Soutar, and B. Vijaya Kumar, "High-speed fingerprint verification using an optical correlator," in Proceedings SPIE, vol. 3386, pp. 123–133, 1998.
5. A. M. Bazen, G. T. B. Verwaaijen, S. H. Gerez, L. P. J. Veelenturf, and B. J. van der Zwaag, "A correlation-based fingerprint verification system," in Proceedings of the ProRISC2000 Workshop on Circuits, Systems and Signal Processing, (Veldhoven, Netherlands), Nov 2000.
6. D. Maio and D. Maltoni, "Direct gray-scale minutiae detection in fingerprints," IEEE Transactions on PAMI, vol. 19, pp. 27–40, Jan 1997.
7. N. K. Ratha and R. M. Bolle, "Effect of controlled acquisition on fingerprint matching," in Proceedings of the International Conference on Pattern Recognition, vol. 2, (Brisbane, Australia), pp. 1659–1661, 1998.
8. C. Dorai, N. Ratha, and R. Bolle, "Detecting dynamic behavior in compressed fingerprint videos: Distortion," in Proceedings of Computer Vision and Pattern Recognition, pp. 320–326, Jun 2000.
9. L. R. Thebaud, "Systems and methods with identity verification by comparison and interpretation of skin patterns such as fingerprints," US Patent 5,909,501, 1999.

ISSN 1512-1232

10. A. M. Bazen and S. Gerez, "Fingerprint matching by thin-plate spline modelling of elastic deformations," Pattern Recognition, vol. 36, pp. 1859–1867, August 2003.
11. A. Senior and R. Bolle, "Improved fingerprint matching by distortion removal," IEICE Transactions on Information and Systems, vol. E84-D, pp. 825–831, Jul 2001.
12. C. Watson, P. Grother, and D. Cassasent, "Distortion-tolerant filter for elastic-distorted fingerprint matching," in Proceedings of SPIE Optical Pattern Recognition, pp. 166–174, 2000.
13. R. Cappelli, D. Maio, and D. Maltoni, "Modelling plastic distortion in fingerprint images," in Proceedings of the Second International Conference on Advances in Pattern Recognition (ICAPR), (Rio de Janeiro), Mar 2001.
14. R. Cappelli, R. Erol, D. Maio, and D. Maltoni, "Synthetic fingerprint-image generation," in Proceedings of the 15th International Conference on Pattern Recognition (ICPR), vol. 3, (Barcelona, Spain), Sep 2000.
15. D. J. Burr, "A dynamic model for image registration," Computer Graphics and Image Processing, vol. 15, pp. 102–112, 1981.
16. L. Younes, "Optimal matching between shapes via elastic deformations," Image and Vision Computing, vol. 17, pp. 381–389, 1999.
17. J. L. Barron, D. J. Fleet, and S. S. Beauchemin, "Performance of optical flow techniques," International Journal Computer Vision, vol. 12, pp. 43–77, 1994.
18. G. E. Christensen, R. D. Rabbitt, and M. I. Miller, "Deformable templates using large deformation kinetics," IEEE Transactions on Image Processing, vol. 5, pp. 1435–1447, 1996.
19. S. C. Joshi and M. I. Miller, "Landmark matching via large deformation diffeo-morphisms," IEEE Transactions on Pattern Analysis and Machine Intelligence, vol. 9, pp. 1357–1370, 2000.
20. Y. Amit, U. Grenander, and M. Piccioni, "Structural image restoration through deformable templates," Journal of American Statistical Association, vol. 86, pp. 376–387, 1991.
21. J. M. Cartensen, "An active lattice model in a Bayesian framework," Computer Vision and Image Understandng, vol. 63, no. 2, pp. 380–387, 1996.
22. C. A. Glasbey and K. V. Mardia, "A penalized likelihood approach to image warping," Journal of the Royal Statistical Society. Series B. Statistical Methodology, vol.63, no.3, pp.465–514, 2001.
23. F. L. Bookstein, "Principal warps: thin-plate splines and the decomposition of deformations," IEEE Transactions on Pattern Analysis and Machine Intelligence, vol. 11, pp. 567–585, 1989.
24. K. V. Mardia and T. J. Hainsworth, "Image warping and Bayesian reconstruction with gray-level templates," in Statistics and Images: Volume 1 (K. V. Mardia and G. K. Kanji, eds.), pp. 257–280, Carfax, Oxford, 1993.
25. K. V. Mardia, T. J. Hainsworth, and J. F. Haddon, "Deformable templates in image sequences," Proceedings of the International Conference on Pattern Recognition (ICPR), pp. 132–135, 1992.
26. A. Almansa and L. Cohen, "Fingerprint image matching by minimization of a thin-plate energy using a two-step algorithm with auxiliary variables," IEEE Workshop on Appl. of Comp. Vision (WACV '00), pp. 35–40, December 2000.
27. I. L. Dryden and K. V. Mardia, Statistical Shape Analysis. John Wiley and Sons, 1998.
28. D. Maio, D. Maltoni, R. Cappelli, J. L. Wayman, and A. K. Jain, "FVC2002: Fingerprint verification competition," in Proceedings of the International Conference on Pattern Recognition (ICPR), (Quebec City, Canada), pp. 744–747, August 2002.
29. W. Bicz, Z. Gumienny, D. Kosz, and M. Pluta, "Ultrasonic setup for fingerprint patterns detection and evaluation," Acoustical Imaging, vol. 22, 1996.

Article received: 2010-04-20